

Adaptive Total Variation Regularization for Weighted Low-Rank Tensor Sparse Hyperspectral Unmixing

Chenguang Xu

Abstract—Hyperspectral images have a low spatial resolution due to the limitations of satellite imaging equipment, resulting in multiple substances contained in a pixel (mixed pixels). The phenomenon of mixed pixels affects the subsequent analyses and researches on hyperspectral images. To address this problem, we propose a novel hyperspectral unmixing method named adaptive total variation regularization for weighted low-rank tensor sparse hyperspectral unmixing (ATVWLRTSU). This method considers the spatial structural characteristics of different regions in the hyperspectral image by using the adaptive Total Variation (ATV) term, and exploits the abundance low-rank tensor by utilizing weighted nuclear norm in hyperspectral unmixing. Simulation and real experiments show that the proposed method has better performance in terms of both anti-noise and details.

Index Terms— adaptive total variation, low-rank tensor, sparse unmixing, hyperspectral images

I. INTRODUCTION

HYPERSPECTRAL technology has made great progress with the development of remote sensing technology in recent decades [1,2]. Due to limitations of satellite equipment, the spatial resolution of hyperspectral images is relatively low [3-5]. The phenomenon of a low-resolution image containing multiple substances in a single pixel is called mixed pixel [6]. A large number of mixed pixels in hyperspectral images make difficulties for subsequent processing and analysis of hyperspectral images [7,8]. In order to solve this problem, scholars have proposed many unmixing methods [9-11].

Generally speaking, hyperspectral mixing models are divided into two categories: linear mixture models and nonlinear mixture models [12,13]. The nonlinear mixture models usually assume that each mixture pixel in hyperspectral data is combined by multiple endmembers in different proportions through a nonlinear form [14], while the linear mixture models assume that the mixture pixel is mixed by these endmembers through linear form [15]. The nonlinear mixture models can more realistically express the process of hyperspectral image mixing, but they have too many

parameters and are difficult to solve, so they are usually replaced by the linear mixture model which is simple and close to the real solution [16].

In the linear methods, sparse unmixing methods are currently the mainstream hyperspectral unmixing methods [17-19], which make unmixing simpler and more effective through a known spectral library [20]. The variable splitting and augmented Lagrangian for sparse unmixing (SUnSAL) [21] is a classic sparse unmixing method. This method utilizes some prior information such as abundance sum-to-one constraint (ASC) and the abundance non-negativity constraint (ANC) to solve [22]. Considering the correlation of local pixels in abundance images, some scholars [23-25] have added the total variation (TV) regularization term for abundance matrix in the unmixing model, such as the sparse unmixing via variable splitting augmented Lagrangian and TV (SUnSAL-TV) [26] and adaptive total variation regularized for hyperspectral unmixing (SU-ATV) [27]. SUnSAL-TV based on SUnSAL only adds the TV regularization term, while SU-ATV considers the characteristics of different regions in the abundance image with different structures and proposes an adaptive TV (ATV) regularization term. SU-ATV not only takes into account the similarity of local pixels in the image like SUnSAL-TV, but also considers the characteristics of spatial structure changes of abundance. On the other hand, the abundance matrix with higher linear correlations exhibits a low-rank phenomenon [28,29]. According to this characteristic, many algorithms [30-32] added low-rank regularization term into the unmixing models to improve the accuracy of unmixing, such as the alternating direction sparse and low-rank unmixing algorithm (ADSpLRU) [33] and weighted nonlocal low-rank tensor decomposition method for sparse unmixing of hyperspectral images (WNLTDTSU) [30]. WNLTDTSU utilizes both collaborative sparsity and low-rank tensor regularization terms to constrain abundance for tensor sparse unmixing, which better protects the structural information of the hyperspectral images. Shen et al [48] proposed a local global based sparse regression unmixing method (LGSU) based on the fact that hyperspectral has local sparsity, thus improving the unmixing performance considering only global sparsity. Later, considering the idea of interactive learning of multilayer abundance matrices, proposed a layered sparse regression decomposition (LSU) [49] to further improve the unmixing accuracy.

However, the above methods only constrain the abundance

Manuscript received June 27, 2024; revised October 3, 2024.

This work was supported in part by Jiangxi Provincial Postgraduate Innovation Special Funds Project (YC2024-B200), in part by Jiangxi Provincial Science and Technology Department of Major Science and Technology R&D Special Project under the "Unveiling and Leading" System (20213AAG01012).

Chenguang Xu is a lecturer of School of Information Engineering, Nanchang Institute of Technology, Nanchang 330099, Jiangxi, China (e-mail: xcg@nit.edu.cn).

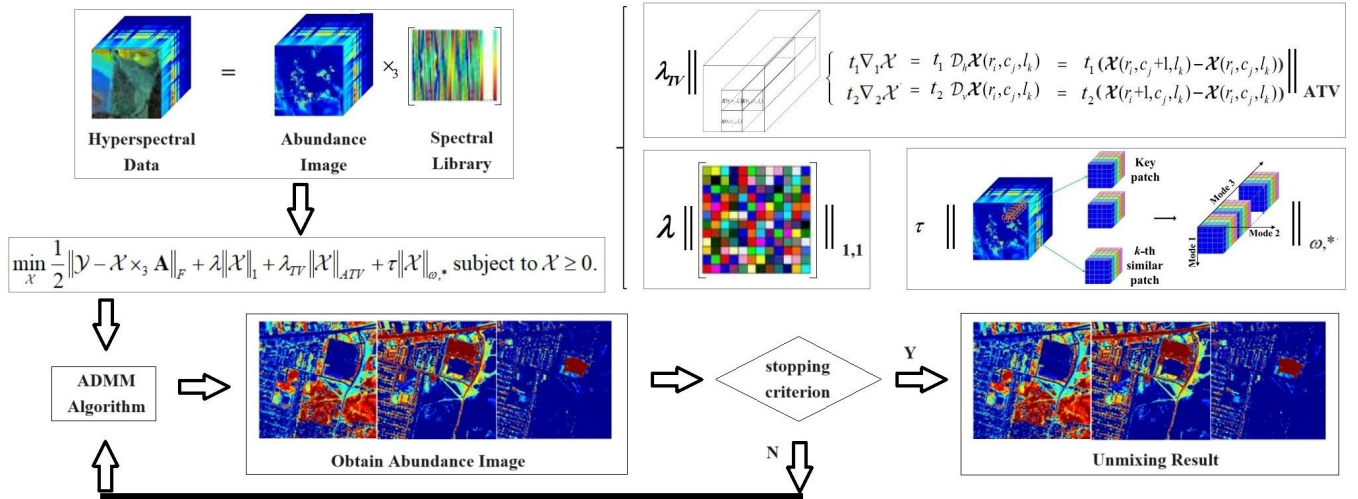


Fig. 1. Flow chart of the proposed ATVWLRTSU method.

matrix through TV, low-rank, abundance weighted, or their variations, ignoring the full utilization of the spatial and spectral information. In order to solve this problem and improve the accuracy of unmixing, a novel hyperspectral unmixing method named adaptive total variation regularization for weighted low-rank tensor sparse hyperspectral unmixing (ATVWLRTSU) is proposed in this study. Fig. 1 presents the flow chart for the ATVWLRTSU. This method considers local similarity by adaptive TV (ATV) regularization term [27] and spatial correlation by nonlocal low-rank tensor regularization term [30]. The three contributions of this article are as follows:

1) According to the spatial structure of the abundance tensor, an adaptive weight matrix is added to the TV regularization item for adjusting the proportion of horizontal and vertical weights in TV. It enables the spatial information of hyperspectral datas to be fully explored.

2) By utilizing the adaptive TV, weighted nuclear norm of abundance tensor and sparse regularization terms, the proposed method simultaneously considers adaptive spatial structure, nonlocal low-rank tensor and sparsity to improve the denoising performance of the unmixing method and enhance the unmixing effect.

3) Efficient solution of the proposed model uses an alternating direction method of multipliers (ADMM) [34].

In section II, we give some introduction to the related work, such as tensor notations and hyperspectral sparse unmixing. In section III, we focus on the contributions of this paper. Firstly, the model of ATVWLRTSU is explained in detail. Secondly, we use the ADMM to solve this model. In section IV, Synthetic and real data experiments are used to validate the state-of-the-art of model ATVWLRTSU. Section V is a summary of the whole paper.

II. RELATED WORK

A. Tensor Notation

Tensor is the symbol used in our algorithm [35]. Let $\mathcal{T} \in \mathbb{R}^{i_1 \times i_2 \times \dots \times i_n}$ ($n > 2$) is a n -dimensional tensor, composed of $i_1 \times i_2 \times \dots \times i_n$ members $\mathcal{T}_{i_1, i_2, \dots, i_n}$, where n is the modes of tensor. An hyperspectral image is usually considered to be three-dimensional (3-D) cubes [36] and can be represented

by 3-D tensor $\mathcal{R} \in \mathbb{R}^{n_1 \times n_2 \times l}$, where n_1 and n_2 are the numbers of hyperspectral pixels, l is the number of spectral bands. Some operations [37] of 3-D tensors is as follows:

Definition 1, Frobenius Norms of 3-D tensors: Given a tensor $\mathcal{R} \in \mathbb{R}^{n_1 \times n_2 \times l}$, its Frobenius norm is defined as $\|\mathcal{R}\|_F = \sqrt{\sum_{i_1=1}^{n_1} \sum_{i_2=1}^{n_2} \sum_{i_3=1}^l |\mathcal{R}_{i_1, i_2, i_3}|^2}$, and its l_1 norm is defined as $\|\mathcal{R}\|_1 = \sum_{i_1=1}^{n_1} \sum_{i_2=1}^{n_2} \sum_{i_3=1}^l |\mathcal{R}_{i_1, i_2, i_3}|$.

Definition 2, Inner product of 3-D tensors: Given two tensor $\mathcal{X} \in \mathbb{R}^{n_1 \times n_2 \times l}$ and $\mathcal{R} \in \mathbb{R}^{n_1 \times n_2 \times l}$. $\langle \mathcal{X}, \mathcal{R} \rangle = \sum_{i_1=1}^{n_1} \sum_{i_2=1}^{n_2} \sum_{i_3=1}^l (\mathcal{X}_{i_1, i_2, i_3} \mathcal{R}_{i_1, i_2, i_3})$ is their inner product expression.

Definition 3, Outer product of m-dimensional tensors: Given two tensors $\mathcal{A} \in \mathbb{R}^{i_1 \times i_2 \times \dots \times i_m}$ and $\mathcal{B} \in \mathbb{R}^{j_1 \times j_2 \times \dots \times j_n}$. Their outer product expression is $\mathcal{Z} = \mathcal{A} \otimes \mathcal{B} \in \mathbb{R}^{i_1 \times i_2 \times \dots \times i_m \times j_1 \times j_2 \times \dots \times j_n}$.

Definition 4, The m-order product: Given a tensor $\mathcal{B} \in \mathbb{R}^{j_1 \times \dots \times j_m \times \dots \times j_n}$ and a matrix $\mathbf{C} \in \mathbb{R}^{i_m \times j_m}$. Their m-order product expression is $\mathcal{Z} = \mathcal{B} \times_m \mathbf{C} \in \mathbb{R}^{j_1 \times \dots \times j_{m-1} \times i_m \times j_{m+1} \times \dots \times j_n}$.

Definition 5, Mode-m unfolding and folding: Given a tensor $\mathcal{B} \in \mathbb{R}^{j_1 \times \dots \times j_m \times \dots \times j_n}$. The Mode-m ($m \in 1, 2, \dots, n$) unfolding of \mathcal{B} is $\mathbf{B}_{(m)} \in \mathbb{R}^{j_m \times (j_1 \times j_2 \times \dots \times j_{m-1} \times j_{m+1} \times \dots \times j_n)}$ and the reverse operation is $\mathcal{B} = \text{fold}_m(\mathbf{B}_{(m)})$ where $\text{fold}_m(\cdot)$ is the inverse function of unfolding. In this article, Mode-third tensors are used, and for simplicity, $\mathbf{B}_{(m)}$ is used instead of $\mathbf{B}_{(3)}$.

B. Hyperspectral sparse unmixing

The hyperspectral linear spectral unmixing model is as follows:

$$\mathbf{Y} = \mathbf{A}\mathbf{X} + \mathbf{N}, \quad (1)$$

where $\mathbf{Y} \in \mathbb{R}^{l \times n}$ is hyperspectral observation data. $\mathbf{X} \in \mathbb{R}^{p \times n}$ represents the abundance matrix corresponding

to spectral library $\mathbf{A} \in \mathbb{R}^{l \times p}$. $\mathbf{N} \in \mathbb{R}^{l \times n}$ represents the noise of the hyperspectral image. l , n and p represent the number of spectral bands, pixels, and different endmembers in the spectral library, respectively.

Sparse unmixing is currently a widely used and effective method for hyperspectral unmixing [38]. It uses a spectral library composed of hundreds of known spectral of different substances as a prior condition [39]. Since the 0-norm can measure the number of non-zero elements in a matrix, the sparsity of the matrix is denoted by $\|\cdot\|_0$ [40]. Due to $\|\cdot\|_0$ is hard to solve, BioucasDias [21] proposed using $\|\cdot\|_1$ to approximately replace $\|\cdot\|_0$ and solving using the SUnSAL method. This model added two constraints, ASC and ANC, to hyperspectral sparse unmixing. The unmixing model is as follows:

$$\min_{\mathbf{X}} \frac{1}{2} \|\mathbf{Y} - \mathbf{A}\mathbf{X}\|_F + \lambda \|\mathbf{X}\|_{1,1}, \text{ subject to } \mathbf{X} \geq 0, \quad (2)$$

where λ is regularization parameter, used to adjust the proportion of approximation term $\|\mathbf{Y} - \mathbf{A}\mathbf{X}\|_F$ and sparsity term $\|\mathbf{X}\|_{1,1}$.

Since SUnSAL ignores the spatial information in hyperspectral, Iordache [26] then proposed an improved method SUnSAL-TV. It is modeled by adding a TV regularization term to the SUnSAL model, which has a constraint function on the spatial information of abundance. The model is as follows:

$$\min_{\mathbf{X}} \|\mathbf{Y} - \mathbf{A}\mathbf{X}\|_F + \lambda \|\mathbf{X}\|_{1,1} + \lambda_{TV} \|\mathbf{X}\|_{TV}, \quad (3)$$

subject to $\mathbf{X} \geq 0$,

where $\|\mathbf{X}\|_{TV} = \left\| \begin{pmatrix} \nabla_1 \mathbf{X} \\ \nabla_2 \mathbf{X} \end{pmatrix} \right\|_{1,1}, \quad \mathbf{X} \in \mathbb{R}^{p \times n},$

$\nabla_1 \mathbf{X} = [h_1, h_2, \dots, h_n]$ and $\nabla_2 \mathbf{X} = [v_1, v_2, \dots, v_n]$ represent horizontal and vertical differences, respectively. $h_i = x_i - x_{ih}$ and $v_j = x_j - x_{jv}$ denote the differences between i pixel and its horizontal neighbour and between j pixel and its vertical neighbour, respectively. $ih \in [1, p]$ and $jv \in [1, n]$. λ_{TV} is regularization parameter, adjusts the proportion of approximation term $\|\mathbf{Y} - \mathbf{A}\mathbf{X}\|_F$, sparsity term $\|\mathbf{X}\|_{1,1}$, and TV term $\|\mathbf{X}\|_{TV}$.

The vectors in the abundance are highly correlated with each other and the abundance matrix consisting of these vectors is low-rank. Giampouras [33] proposed the ADSpLRU method, which improves the unmixing accuracy by adding a nuclear norm regularization term to constrain the low-rank abundance.

$$\min_{\mathbf{X}} \|\mathbf{Y} - \mathbf{A}\mathbf{X}\|_F + \lambda \|\mathbf{X}\|_{1,1} + \tau \|\mathbf{X}\|_{b,*}, \quad (4)$$

subject to $\mathbf{X} \geq 0$,

where

$$\|\mathbf{X}\|_{b,*} = \sum_{i=1}^{rank(\mathbf{X})} b_i \sigma_i(\mathbf{X}), \quad b_i = 1/(\sigma_i(\mathbf{X}) + \varepsilon)$$

and $\sigma_i(\mathbf{X})$ is the singular values of \mathbf{X} . ε is the smallest non-negative value. $rank(\mathbf{X})$ is the rank of \mathbf{X} . τ is regularization parameter of low rank term.

A hyperspectral image is a 3-D cube composed of continuous bands of many different substances [41]. The traditional 2-D hyperspectral image that vectorizes the abundance images according to the spectral dimensions, loses a lot of spatial information compared to 3-D hyperspectral images cube [42]. The sparse unmixing model is:

$$\mathcal{Y} = \mathcal{X} \times_3 \mathbf{A} + \mathcal{N}, \quad (5)$$

where $\mathcal{Y} = fold_3(\mathbf{Y}_{(3)}) \in \mathbb{R}^{n_1 \times n_2 \times l}$ and $\mathcal{X} = fold_3(\mathbf{X}_{(3)}) \in \mathbb{R}^{n_1 \times n_2 \times p}$ are tensor forms of hyperspectral images $\mathbf{Y}_{(3)}$ and $\mathbf{X}_{(3)}$ respectively. $n_1 \times n_2 = n$. In this article, we use \mathbf{X} simplification to represent $\mathbf{X}_{(3)}$ and \mathcal{Y} simplification to represent $\mathbf{Y}_{(3)}$. \mathcal{Y} is 3-D hyperspectral observation data. \mathcal{X} represents the abundance tensor. $\mathbf{A} \in \mathbb{R}^{l \times p}$ is spectral library. $\mathcal{N} \in \mathbb{R}^{n_1 \times n_2 \times l}$ represents the 3-D noise of the hyperspectral image.

Le Sun [30] proposed the WNLTDSU method, which takes the hyperspectral image tensor as the unmixing object, and integrates TV and low-rank tensor regularization terms to significantly improve the unmixing results. The sparse unmixing optimization problem is:

$$\min_{\mathcal{X}} \frac{1}{2} \|\mathcal{Y} - \mathcal{X} \times_3 \mathbf{A}\|_F + \lambda \|\mathcal{X}\|_{2,1} + \lambda_{TV} \|\mathcal{X}\|_{TV} + \tau \|\mathcal{X}\|_{\omega,*}, \quad (6)$$

subject to $\mathcal{X} \geq 0$,

where $\|\mathcal{X}\|_{2,1} = \|\mathbf{X}_{(3)}\|_{2,1} = \sum_{i=1}^p \sqrt{\sum_{j=1}^n x_{ij}^2}$, $\mathbf{X}_{(3)} \in \mathbb{R}^{p \times n}$. $\|\mathcal{X}\|_{TV} = \left\| \begin{pmatrix} \nabla_1 \mathcal{X} \\ \nabla_2 \mathcal{X} \end{pmatrix} \right\|_{1,1}$, and $\nabla_1 \mathcal{X}(i, j, k) = \mathcal{X}(i, j + l, k) - \mathcal{X}(i, j, k)$, $\nabla_2 \mathcal{X}(i, j, k) = \mathcal{X}(i + 1, j, k) - \mathcal{X}(i, j, k)$ represent horizontal and vertical differences operators, respectively, $i = 1, 2, \dots, n_1$, $j = 1, 2, \dots, n_2$ and $k = 1, 2, \dots, l$.

$\|\mathcal{X}\|_{\omega,*} = \sum_{q=1}^Q \|\mathcal{X}_q\|_{\omega,*} = \sum_{q=1}^Q \|\mathbf{X}_{(3)}^q\|_{\omega,*} = \sum_{q=1}^Q \sum_{j=1}^{rank(\mathbf{X}_{(3)}^q)} \omega_j \sigma_j(\mathbf{X}_{(3)}^q)$, \mathcal{X}_q is a 3-D non-local similar patch in \mathcal{X} , which is composed of many similar 3-D local patches in different regions of \mathcal{X} . Q represents the number of non-local patches in \mathcal{X} . $\omega_j = d \sqrt{k+1} / (\sigma_j(\mathbf{X}_{(3)}^q) + \varepsilon)$, where d is a constant greater than zero and k is the number of similar patches.

III. PROPOSED METHOD

TABLE I
The pseudocode of ATVWLRTSU

Algorithm 1: ATVWLRTSU algorithm

1. Choose: $\mu > 0$, $\lambda > 0$, $\lambda_{TV} > 0$, $\tau > 0$, $k > 0$,
and set $i = 0$,
 $\mathcal{X}^{(0)} = [\mathcal{Y} \times_3 \mathbf{A}^T] \times_3 (\mathbf{A}\mathbf{A}^T + 4\mathbf{I})^{-1}$,
 $\mathcal{V}_1^{(0)} = \mathcal{X}^{(0)} \times_3 \mathbf{A}$, $\mathcal{V}_2^{(0)} = \mathcal{X}^{(0)}$, $\mathcal{V}_3^{(0)} = \mathcal{X}^{(0)}$,
 $\mathcal{V}_4^{(0)} = \nabla \mathcal{V}_3^{(0)}$, $\mathcal{V}_5^{(0)} = T\mathcal{V}_4^{(0)}$, $\mathcal{V}_6^{(0)} = \mathcal{X}^{(0)}$, $\mathcal{V}_7^{(0)} = \mathcal{X}^{(0)}$,
 $\mathcal{D}_1^{(0)} = \mathcal{D}_2^{(0)} = \mathcal{D}_3^{(0)} = \mathcal{D}_4^{(0)} = \mathcal{D}_5^{(0)} = \mathcal{D}_6^{(0)} = \mathcal{D}_7^{(0)} = 0$,
 $t_1^{(0)} = 1 / \left(1 + k |G_{\delta} * \nabla_1 \mathcal{X}^{(0)}|^2 \right)$,
 $t_2^{(0)} = 1 / \left(1 + k |G_{\delta} * \nabla_2 \mathcal{X}^{(0)}|^2 \right)$.
2. Repeat
 - (1) Update variables:
 - (a) $\mathcal{X}^{(i+1)} = \arg \min_{\mathcal{X}} \frac{\mu}{2} \|\mathcal{X} \times_3 \mathbf{A} - \mathcal{V}_1^{(i)} - \mathcal{D}_1^{(i)}\|_F^2$
 $+ \frac{\mu}{2} \|\mathcal{X} - \mathcal{V}_2^{(i)} - \mathcal{D}_2^{(i)}\|_F^2 + \frac{\mu}{2} \|\mathcal{X} - \mathcal{V}_3^{(i)} - \mathcal{D}_3^{(i)}\|_F^2$
 $+ \frac{\mu}{2} \|\mathcal{X} - \mathcal{V}_6^{(i)} - \mathcal{D}_6^{(i)}\|_F^2 + \frac{\mu}{2} \|\mathcal{X} - \mathcal{V}_7^{(i)} - \mathcal{D}_7^{(i)}\|_F^2$,
 $\mathcal{V}_1^{(i+1)} = \arg \min_{\mathcal{V}_1} \frac{1}{2} \|\mathcal{Y} - \mathcal{V}_1\|_F^2$
 $+ \frac{\mu}{2} \|\mathcal{X}^{(i+1)} \times_3 \mathbf{A} - \mathcal{V}_1 - \mathcal{D}_1^{(i)}\|_F^2$.
 - (b) $\mathcal{V}_2^{(i+1)} = \arg \min_{\mathcal{V}_2} \lambda \|\mathcal{V}_2\|_{1,1}$
 - (c) $+ \frac{\mu}{2} \|\mathcal{X}^{(i+1)} - \mathcal{V}_2 - \mathcal{D}_2^{(i)}\|_F^2$.
 - (d) $\mathcal{V}_3^{(i+1)} = \arg \min_{\mathcal{V}_3} \frac{\mu}{2} \|\mathcal{X}^{(i+1)} - \mathcal{V}_3 - \mathcal{D}_3^{(i)}\|_F^2$
 $+ \frac{\mu}{2} \|\nabla \mathcal{V}_3 - \mathcal{V}_4 - \mathcal{D}_4^{(i)}\|_F^2$.
 - (e) $\mathcal{V}_4^{(i+1)} = \arg \min_{\mathcal{V}_4} \frac{\mu}{2} \|\nabla \mathcal{V}_3^{(i+1)} - \mathcal{V}_4 - \mathcal{D}_4^{(i)}\|_F^2$
 $+ \frac{\mu}{2} \|T\mathcal{V}_4 - \mathcal{V}_5 - \mathcal{D}_5^{(i)}\|_F^2$.
 - (f) $\mathcal{V}_5^{(i+1)} = \arg \min_{\mathcal{V}_5} \lambda_{TV} \|\mathcal{V}_5\|_{2,1}$
 - (g) $+ \frac{\mu}{2} \|T\mathcal{V}_4^{(i+1)} - \mathcal{V}_5 - \mathcal{D}_5^{(i)}\|_F^2$
 $\mathcal{V}_6^{(i+1)} = \arg \min_{\mathcal{V}_6} \tau \|\mathcal{V}_6\|_{\omega,*}$
 - (h) $+ \frac{\mu}{2} \|\mathcal{X}^{(i+1)} - \mathcal{V}_6 - \mathcal{D}_6^{(i)}\|_F^2$
 $\mathcal{V}_7^{(i+1)} = \arg \min_{\mathcal{V}_7} i - R_+(\mathcal{V}_7)$
 - (i) $+ \frac{\mu}{2} \|\mathcal{X}^{(i+1)} - \mathcal{V}_7 - \mathcal{D}_7^{(i)}\|_F^2$.
 - (2) Update Lagrangian operator:
 - (i) $\mathcal{D}_1^{(i+1)} = \mathcal{D}_1^{(i)} - \left(\mathcal{X}^{(i+1)} \times_3 \mathbf{A} - \mathcal{V}_1^{(i+1)} \right)$,
 - (j) $\mathcal{D}_2^{(i+1)} = \mathcal{D}_2^{(i)} - \left(\mathcal{X}^{(i+1)} - \mathcal{V}_2^{(i+1)} \right)$,
 - (k) $\mathcal{D}_3^{(i+1)} = \mathcal{D}_3^{(i)} - \left(\mathcal{X}^{(i+1)} - \mathcal{V}_3^{(i+1)} \right)$,
 - (l) $\mathcal{D}_4^{(i+1)} = \mathcal{D}_4^{(i)} - \left(\nabla \mathcal{V}_3^{(i+1)} - \mathcal{V}_4^{(i+1)} \right)$,
 - (m) $\mathcal{D}_5^{(i+1)} = \mathcal{D}_5^{(i)} - \left(T\mathcal{V}_4^{(i+1)} - \mathcal{V}_5^{(i+1)} \right)$.
 - (n) $\mathcal{D}_6^{(i+1)} = \mathcal{D}_6^{(i)} - \left(\mathcal{X}^{(i+1)} - \mathcal{V}_6^{(i+1)} \right)$,
 - (o) $\mathcal{D}_7^{(i+1)} = \mathcal{D}_7^{(i)} - \left(\mathcal{X}^{(i+1)} - \mathcal{V}_7^{(i+1)} \right)$.
 - (3) Replacement of variate:
 - (p) $t_1^{(i)} = 1 / \left(1 + k |G_{\delta} * \nabla_1 \mathcal{X}^{(i)}|^2 \right)$.
 - (q) $t_2^{(i)} = 1 / \left(1 + k |G_{\delta} * \nabla_2 \mathcal{X}^{(i)}|^2 \right)$.
 - (4) Update iterations: $i = i + 1$.
3. Until a certain stopping criterion is satisfied.

(2) Update Lagrangian operator:

- (i) $\mathcal{D}_1^{(i+1)} = \mathcal{D}_1^{(i)} - \left(\mathcal{X}^{(i+1)} \times_3 \mathbf{A} - \mathcal{V}_1^{(i+1)} \right)$,
- (j) $\mathcal{D}_2^{(i+1)} = \mathcal{D}_2^{(i)} - \left(\mathcal{X}^{(i+1)} - \mathcal{V}_2^{(i+1)} \right)$,
- (k) $\mathcal{D}_3^{(i+1)} = \mathcal{D}_3^{(i)} - \left(\mathcal{X}^{(i+1)} - \mathcal{V}_3^{(i+1)} \right)$,
- (l) $\mathcal{D}_4^{(i+1)} = \mathcal{D}_4^{(i)} - \left(\nabla \mathcal{V}_3^{(i+1)} - \mathcal{V}_4^{(i+1)} \right)$,
- (m) $\mathcal{D}_5^{(i+1)} = \mathcal{D}_5^{(i)} - \left(T\mathcal{V}_4^{(i+1)} - \mathcal{V}_5^{(i+1)} \right)$.
- (n) $\mathcal{D}_6^{(i+1)} = \mathcal{D}_6^{(i)} - \left(\mathcal{X}^{(i+1)} - \mathcal{V}_6^{(i+1)} \right)$,
- (o) $\mathcal{D}_7^{(i+1)} = \mathcal{D}_7^{(i)} - \left(\mathcal{X}^{(i+1)} - \mathcal{V}_7^{(i+1)} \right)$.

(3) Replacement of variate:

- (p) $t_1^{(i)} = 1 / \left(1 + k |G_{\delta} * \nabla_1 \mathcal{X}^{(i)}|^2 \right)$.
- (q) $t_2^{(i)} = 1 / \left(1 + k |G_{\delta} * \nabla_2 \mathcal{X}^{(i)}|^2 \right)$.

(4) Update iterations: $i = i + 1$.

3. Until a certain stopping criterion is satisfied.

A. Adaptive Total Variation Regularization

The TV regularization term has the same proportion of horizontal differences $\nabla_1 \mathcal{X}$ and vertical differences $\nabla_2 \mathcal{X}$. However, different regions in hyperspectral images have different structures, and the horizontal and vertical proportions of the tangent line along theregion's edges are different [43-44]. It is important to maintain the diffusion of the corresponding Euler-Lagrange equation in the tangent direction of the image edge [45]. The adaptive total variation (ATV) regularization term is as follows:

$$\|\mathcal{X}\|_{ATV} = \|T\nabla \mathcal{X}\|_{2,1}, \quad (7)$$

where $\nabla \mathcal{X} = \begin{pmatrix} \nabla_1 \mathcal{X} \\ \nabla_2 \mathcal{X} \end{pmatrix}$, $T = \begin{pmatrix} t_1 & 0 \\ 0 & t_2 \end{pmatrix}$ is a weight matrix

and $t_1 = 1 / \left(k |G_{\delta} * \nabla_1 \mathcal{X}|^2 \right)$ and $t_2 = 1 / \left(k |G_{\delta} * \nabla_2 \mathcal{X}|^2 \right)$ are the weight coefficients of $\nabla_1 \mathcal{X}$ and $\nabla_2 \mathcal{X}$, respectively.

k and δ are the tuning parameters, G_{δ} represents the Gaussian convolutional kernel, and $*$ is the convolution operator. $(\bullet)^2$ denotes a new 3-D tensor obtained by squaring each element in the 3-D tensor (\bullet) .

$$\|\mathcal{X}\|_{ATV} = \left\| \begin{pmatrix} t_1 & 0 \\ 0 & t_2 \end{pmatrix} \begin{pmatrix} \nabla_1 \mathcal{X} \\ \nabla_2 \mathcal{X} \end{pmatrix} \right\|_{2,1} = \left\| \begin{pmatrix} t_1 \nabla_1 \mathcal{X} \\ t_2 \nabla_2 \mathcal{X} \end{pmatrix} \right\|_{2,1} \quad (8)$$

$$= \left\| \sqrt{(t_1 \nabla_1 \mathcal{X})^2 + (t_2 \nabla_2 \mathcal{X})^2} \right\|_1,$$

B. Proposed Model and Optimization

An novel sparse unmixing model after adding the ATV, sparse tensor and weighted low-rank tensor regularization terms is named adaptive total variation regularization for weighted low-rank tensor sparse unmixing model (ATVWLRTSU) as follows:

$$\min_{\mathcal{X}} \frac{1}{2} \|\mathcal{Y} - \mathcal{X} \times_3 \mathbf{A}\|_F + \lambda \|\mathcal{X}\|_1 + \lambda_{TV} \|\mathcal{X}\|_{ATV} + \tau \|\mathcal{X}\|_{\omega,*},$$

subject to $\mathcal{X} \geq 0$.

(9)

Expand and write the above equation as:

$$\min_{\mathcal{X}} \frac{1}{2} \|\mathcal{Y} - \mathcal{X} \times_3 \mathbf{A}\|_F + \lambda \|\mathcal{X}\|_1 + \lambda_{TV} \|\nabla \mathcal{X}\|_{2,1} + \tau \|\mathcal{X}\|_{\omega,*},$$

subject to $\mathcal{X} \geq 0$.

(10)

where $\|\mathcal{Y} - \mathcal{X} \times_3 \mathbf{A}\|_F^2$ is a data fitting term to make the unmixing result more close to the real value; $\|\mathcal{X}\|_1 = \sum_{i=1}^{n_1} \sum_{j=1}^{n_2} \sum_{k=1}^l x_{i,j,k}$ is a sparsity constraint term used to constrain the abundance sparsity during the unmixing process; $\|\nabla \mathcal{X}\|_{2,1}$ is an adaptive TV term used to adaptively adjust the weights of the horizontal and vertical differences of the abundance under different structures in each iteration to achieve a better denoising effect; $\|\mathcal{X}\|_{\omega,*}$ is a low-rank term used to de-correlate the abundance to make the result more robust; $\mathcal{X} \geq 0$. is a non-negativity constraint on abundance. λ , λ_{TV} , τ are regularisation parameters to adjust the weight ratio of the sparse constraint term, the adaptive TV constraint term and the low-rank constraint term.

In order to solve the above problem, we used the alternating direction method of multipliers (ADMM) [34] for solving this problem. Using ADMM, formula (9) can be converted to:

$$\min_{\mathcal{X}} \frac{1}{2} \|\mathcal{Y} - \mathcal{V}_1\|_F + \lambda \|\mathcal{V}_2\|_1 + \lambda_{TV} \|\mathcal{V}_5\|_{2,1} + \tau \|\mathcal{V}_6\|_{\omega,*} + i_{R_+}(\mathcal{V}_7)$$

(11)

where $\mathcal{V}_1 = \mathcal{X} \times_3 \mathbf{A}$, $\mathcal{V}_2 = \mathcal{X}$, $\mathcal{V}_3 = \mathcal{X}$, $\mathcal{V}_4 = \nabla \mathcal{V}_3$, $\mathcal{V}_5 = TV \mathcal{V}_4$, $\mathcal{V}_6 = \mathcal{X}$, $\mathcal{V}_7 = \mathcal{X}$ and $i_{R_+}(\mathcal{X})$ represents $\mathcal{X} \geq 0$.

The Lagrangian function can be written as:

$$\zeta \left(\begin{matrix} \mathcal{X}, \mathcal{V}_1, \mathcal{V}_2, \mathcal{V}_3, \mathcal{V}_4, \mathcal{V}_5, \mathcal{V}_6, \mathcal{V}_7 \\ \mathcal{D}_1, \mathcal{D}_2, \mathcal{D}_3, \mathcal{D}_4, \mathcal{D}_5, \mathcal{D}_6, \mathcal{D}_7 \end{matrix} \right) =$$

$$\min_{\mathcal{X}} \frac{1}{2} \|\mathcal{Y} - \mathcal{V}_1\|_F^2 + \lambda \|\mathcal{V}_2\|_1 + \lambda_{TV} \|\mathcal{V}_5\|_{2,1} + \tau \|\mathcal{V}_6\|_{\omega,*}$$

$$+ i_{R_+}(\mathcal{V}_7) + \frac{\mu}{2} \|\mathcal{X} \times_3 \mathbf{A} - \mathcal{V}_1 - \mathcal{D}_1\|_F^2 +$$

$$\frac{\mu}{2} \|\mathcal{X} - \mathcal{V}_2 - \mathcal{D}_2\|_F^2 + \frac{\mu}{2} \|\mathcal{X} - \mathcal{V}_3 - \mathcal{D}_3\|_F^2 +$$

$$\frac{\mu}{2} \|\nabla \mathcal{V}_3 - \mathcal{V}_4 - \mathcal{D}_4\|_F^2 + \frac{\mu}{2} \|TV \mathcal{V}_4 - \mathcal{V}_5 - \mathcal{D}_5\|_F^2 +$$

$$\frac{\mu}{2} \|\mathcal{X} - \mathcal{V}_6 - \mathcal{D}_6\|_F^2 + \frac{\mu}{2} \|\mathcal{X} - \mathcal{V}_7 - \mathcal{D}_7\|_F^2,$$

(12)

where $\mathcal{D}_1, \mathcal{D}_2, \mathcal{D}_3, \mathcal{D}_4, \mathcal{D}_5, \mathcal{D}_6, \mathcal{D}_7$ are Lagrangian multipliers, and $\mu > 0$ is Lagrangian penalty factor.

We iteratively solve $\mathcal{X}, \mathcal{V}_1, \mathcal{V}_2, \mathcal{V}_3, \mathcal{V}_4, \mathcal{V}_5, \mathcal{V}_6, \mathcal{V}_7$ and $\mathcal{D}_1, \mathcal{D}_2, \mathcal{D}_3, \mathcal{D}_4, \mathcal{D}_5, \mathcal{D}_6, \mathcal{D}_7$ in sequence, using the ADMM algorithm. The following shows the solution process for several sub-problems:

(1) Sub-problems \mathcal{X} :

$$\mathcal{X}^{(i+1)} = \arg \min_{\mathcal{X}} \frac{\mu}{2} \|\mathcal{X} \times_3 \mathbf{A} - \mathcal{V}_1^{(i)} - \mathcal{D}_1^{(i)}\|_F^2 +$$

$$\frac{\mu}{2} \|\mathcal{X} - \mathcal{V}_2^{(i)} - \mathcal{D}_2^{(i)}\|_F^2 + \frac{\mu}{2} \|\mathcal{X} - \mathcal{V}_3^{(i)} - \mathcal{D}_3^{(i)}\|_F^2$$

$$+ \frac{\mu}{2} \|\mathcal{X} - \mathcal{V}_6^{(i)} - \mathcal{D}_6^{(i)}\|_F^2 + \frac{\mu}{2} \|\mathcal{X} - \mathcal{V}_7^{(i)} - \mathcal{D}_7^{(i)}\|_F^2,$$

(13)

where $(\cdot)^{(i)}$ represents the result of the *ith* iteration of (\cdot) .

By solving we can get:

$$\mathcal{X}^{(i+1)} = \left[\begin{matrix} (\mathcal{V}_1^{(i)} + \mathcal{D}_1^{(i)}) \times_3 \mathbf{A}^T + (\mathcal{V}_2^{(i)} + \mathcal{D}_2^{(i)}) + (\mathcal{V}_3^{(i)}) \\ + \mathcal{D}_3^{(i)} + (\mathcal{V}_6^{(i)} + \mathcal{D}_6^{(i)}) + (\mathcal{V}_7^{(i)} + \mathcal{D}_7^{(i)}) \end{matrix} \right]$$

$$\times_3 (\mathbf{A}\mathbf{A}^T + 4\mathbf{I})^{-1}$$

(14)

where \mathbf{I} represents the identity matrix.

(2) Sub-problems \mathcal{V}_1 :

$$\mathcal{V}_1^{(i+1)} = \arg \min_{\mathcal{V}_1} \frac{1}{2} \|\mathcal{Y} - \mathcal{V}_1\|_F^2 +$$

$$\frac{\mu}{2} \|\mathcal{X}^{(i+1)} \times_3 \mathbf{A} - \mathcal{V}_1 - \mathcal{D}_1^{(i)}\|_F^2.$$

(15)

By solving we can get:

$$\mathcal{V}_1^{(i+1)} = \frac{1}{1+\mu} \mathcal{Y} + \frac{\mu}{1+\mu} (\mathcal{X}^{(i+1)} \times_3 \mathbf{A} - \mathcal{D}_1^{(i)}).$$

(16)

(3) Sub-problems \mathcal{V}_2 :

$$\mathcal{V}_2^{(i+1)} = \arg \min_{\mathcal{V}_2} \lambda \|\mathcal{V}_2\|_{1,1} + \frac{\mu}{2} \|\mathcal{X}^{(i+1)} - \mathcal{V}_2 - \mathcal{D}_2^{(i)}\|_F^2.$$

(17)

By solving we can get:

$$\mathcal{V}_2^{(i+1)} = \text{soft} \left[(\mathcal{X}^{(i+1)} - \mathcal{D}_2^{(i)}), \frac{\lambda}{\mu} \right],$$

(18)

where $\text{soft}(\mathbf{a}, \mathbf{b}) = \text{sgn}(\mathbf{a}) \max(|\mathbf{a}| - \mathbf{b}, 0)$.

(4) Sub-problems \mathcal{V}_3 :

$$\mathcal{V}_3^{(i+1)} = \arg \min_{\mathcal{V}_3} \frac{\mu}{2} \|\mathcal{X}^{(i+1)} - \mathcal{V}_3 - \mathcal{D}_3^{(i)}\|_F^2 +$$

$$\frac{\mu}{2} \|\nabla \mathcal{V}_3 - \mathcal{V}_4^{(i)} - \mathcal{D}_4^{(i)}\|_F^2.$$

(19)

By solving we can get:

$$\mathcal{V}_3^{(i+1)} = \mathcal{F} \left[\frac{\mathcal{F} \left[(\mathcal{X}^{(i+1)} - \mathcal{D}_3^{(i)}) - \text{div}(\mathcal{V}_4^{(i)} + \mathcal{D}_4^{(i)}) \right]}{\mathcal{F}[(\mathbf{I} - \text{div}\nabla)]} \right].$$

(20)

(5) Sub-problems \mathcal{V}_4 :

$$\begin{aligned} \mathcal{V}_4^{(i+1)} = \arg \min_{\mathcal{V}_4} \frac{\mu}{2} \|\nabla \mathcal{V}_3^{(i+1)} - \mathcal{V}_4 - \mathcal{D}_4^{(i)}\|_F^2 + \\ \frac{\mu}{2} \|\mathcal{T}\mathcal{V}_4 - \mathcal{V}_5^{(i)} - \mathcal{D}_5^{(i)}\|_F^2. \end{aligned} \quad (21)$$

By simplifying formula (20), we can obtain:

$$(I + T^2)\mathcal{V}_4^{(i+1)} = (\nabla \mathcal{V}_3^{(i+1)} - \mathcal{D}_4^{(i)}) + T(\mathcal{V}_5^{(i)} + \mathcal{D}_5^{(i)}). \quad (22)$$

Expand formula (22) to obtain:

$$\begin{aligned} \begin{pmatrix} t_1^2 + 1 & 0 \\ 0 & t_2^2 + 1 \end{pmatrix} \begin{pmatrix} \mathcal{V}_{41}^{(i+1)} \\ \mathcal{V}_{42}^{(i+1)} \end{pmatrix} = \begin{pmatrix} \nabla_1 \mathcal{V}_3^{(i+1)} - \mathcal{D}_{41}^{(i)} \\ \nabla_2 \mathcal{V}_3^{(i+1)} - \mathcal{D}_{42}^{(i)} \end{pmatrix} \\ + \begin{pmatrix} t_1 & 0 \\ 0 & t_2 \end{pmatrix} \begin{pmatrix} \mathcal{V}_{51}^{(i)} - \mathcal{D}_{51}^{(i)} \\ \mathcal{V}_{52}^{(i)} - \mathcal{D}_{52}^{(i)} \end{pmatrix}. \end{aligned} \quad (23)$$

Further obtaining:

$$(t_1^2 + 1)\mathcal{V}_{41}^{(i+1)} = (\nabla_1 \mathcal{V}_3^{(i+1)} - \mathcal{D}_{41}^{(i)}) + t_1(\mathcal{V}_{51}^{(i)} - \mathcal{D}_{51}^{(i)}). \quad (24)$$

$$(t_2^2 + 1)\mathcal{V}_{42}^{(i+1)} = (\nabla_2 \mathcal{V}_3^{(i+1)} - \mathcal{D}_{42}^{(i)}) + t_2(\mathcal{V}_{52}^{(i)} - \mathcal{D}_{52}^{(i)}). \quad (25)$$

Finally, we can obtain the results:

$$\mathcal{V}_{41}^{(i+1)} = \frac{1}{t_1^2 + 1} [(\nabla_1 \mathcal{V}_3^{(i+1)} - \mathcal{D}_{41}^{(i)}) + t_1(\mathcal{V}_{51}^{(i)} - \mathcal{D}_{51}^{(i)})]. \quad (26)$$

$$\mathcal{V}_{42}^{(i+1)} = \frac{1}{t_2^2 + 1} [(\nabla_2 \mathcal{V}_3^{(i+1)} - \mathcal{D}_{42}^{(i)}) + t_2(\mathcal{V}_{52}^{(i)} - \mathcal{D}_{52}^{(i)})]. \quad (27)$$

(6) Sub-problems \mathcal{V}_5 :

$$\mathcal{V}_5^{(i+1)} = \arg \min_{\mathcal{V}_5} \lambda_{TV} \|\mathcal{V}_5\|_{2,1} + \frac{\mu}{2} \|\mathcal{T}\mathcal{V}_4^{(i+1)} - \mathcal{V}_5 - \mathcal{D}_5^{(i)}\|_F^2. \quad (28)$$

By solving formula (28), we can obtain:

$$\mathcal{V}_5^{(i+1)} = \text{soft}\left(\mathcal{T}\mathcal{V}_4^{(i+1)} - \mathcal{D}_5^{(i)}, \frac{\lambda_{TV}}{\mu}\right). \quad (29)$$

(7) Sub-problems \mathcal{V}_6 :

$$\mathcal{V}_6^{(i+1)} = \arg \min_{\mathcal{V}_6} \tau \|\mathcal{V}_6\|_{\omega,*} + \frac{\mu}{2} \|\mathcal{X}^{(i+1)} - \mathcal{V}_6 - \mathcal{D}_6^{(i)}\|_F^2. \quad (30)$$

By solving we can get:

$$\mathcal{V}_6^{(i+1)} = \text{soft}\left(\mathcal{X}^{(i+1)} - \mathcal{D}_6^{(i)}, \frac{\tau}{\mu} \omega\right). \quad (31)$$

(8) Sub-problems \mathcal{V}_7 :

$$\mathcal{V}_7^{(i+1)} = \arg \min_{\mathcal{V}_7} i_- R_+(\mathcal{V}_7) + \frac{\mu}{2} \|\mathcal{X}^{(i+1)} - \mathcal{V}_7 - \mathcal{D}_7^{(i)}\|_F^2. \quad (32)$$

By solving we can get:

$$\mathcal{V}_7^{(i+1)} = \max(\mathcal{X}^{(i+1)} - \mathcal{D}_7^{(i)}, 0). \quad (33)$$

During the iterative, \mathcal{X} is update first, then $\mathcal{V}_1, \mathcal{V}_2, \mathcal{V}_3, \mathcal{V}_4, \mathcal{V}_5, \mathcal{V}_6, \mathcal{V}_7$, and finally $\mathcal{D}_1, \mathcal{D}_2, \mathcal{D}_3, \mathcal{D}_4, \mathcal{D}_5, \mathcal{D}_6, \mathcal{D}_7$. Until a certain stopping criterion is satisfied, the iterations do not end. The pseudocode of ATVWLRTSU is shown in TABLE I.

In TABLE I, the algorithm execution process can be

divided into three steps. The first step is the initialisation, in which we initialise the variables and parameters. The second step is the update and loop iteration steps, in which both the requested variables and the intermediate variables are iterated and updated until the set stop conditions are met. The third step is to stop and return the result.

IV. EXPERIMENTS AND ANALYSIS

In this section, we validate the proposed method (ATVWLRTSU) using two synthetic hyperspectral datasets and one real hyperspectral dataset. We compare the unmixing performance of several state-of-the-art methods (SUNSAL-TV [26], SU-ATV [27], ADSpLRU [33], WNLTDUSU [30], LGSU [48], LSU [49]) with the proposed method, and conduct a detailed analysis of the comparison results. These methods are all sparse unmixing algorithms. SUNSAL-TV makes use of a TV regularization term, while SU-ATV comes with an adaptive TV regularization term. ADSpLRU makes use of the low-rank constraint for abundance matrix, while WNLTDUSU has the weighted nonlocal low-rank tensor as prior information. And the proposed method (ATVWLRTSU) combines their advantages by including not only adaptive TV regularization term but also weighted nonlocal low-rank tensor regularization term. LGSU uses locally sparse regular terms for superpixels. LSU utilises a multilayer sparse regression method with interactive learning.

A. Experiments with synthetic data

In the experiment, the signal-to-reconstruction error (SRE), the probability of success (p_s) and *sparsity* are used to evaluate the unmixing accuracy. Their definitions are as follows:

$$\text{SRE(dB)} = 10 \lg \frac{\mathbb{E}(\|\mathcal{X}\|_2^2)}{\mathbb{E}(\|\mathcal{X} - \hat{\mathcal{X}}\|_2^2)}, \quad (34)$$

where $\hat{\mathcal{X}}$ is the estimated value of the true abundance \mathcal{X} , $\mathbb{E}(\cdot)$ represents the expected of (\cdot) . The higher SRE, the smaller the signal reconstruction error, and the better the unmixing effect.

$$p_s = P\left(\frac{\|\mathcal{X} - \hat{\mathcal{X}}\|_2^2}{\|\mathcal{X}\|_2^2} \leq \text{threshold}\right), \quad (35)$$

where $P(\cdot)$ represents the probability that (\cdot) is valid. The *threshold* is a threshold, usually set to 3.16(5dB) [21]. The higher p_s , the higher the probability of success, and the better the unmixing effect.

$$\text{sparsity} = \frac{\|\max(\hat{\mathbf{X}}_{(3)} - 0.005, 0)\|_0}{p \times n_1 \times n_2}, \quad (36)$$

where $\hat{\mathbf{X}}_{(3)} \in \mathbb{R}^{p \times n}$ is Mode-3 unfolding of $\hat{\mathcal{X}} \in \mathbb{R}^{n_1 \times n_2 \times p}$ and $n = n_1 \times n_2$. The lower *sparsity*, the sparser the abundance, and the more accurate the unmixing is.

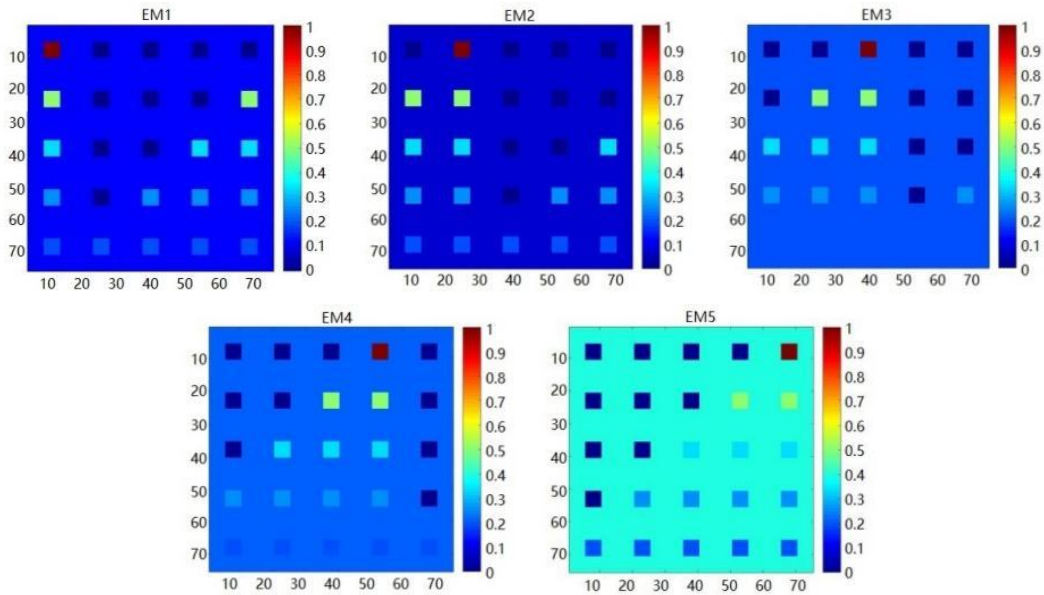


Fig. 2. True abundances of each endmembers in synthetic SD1

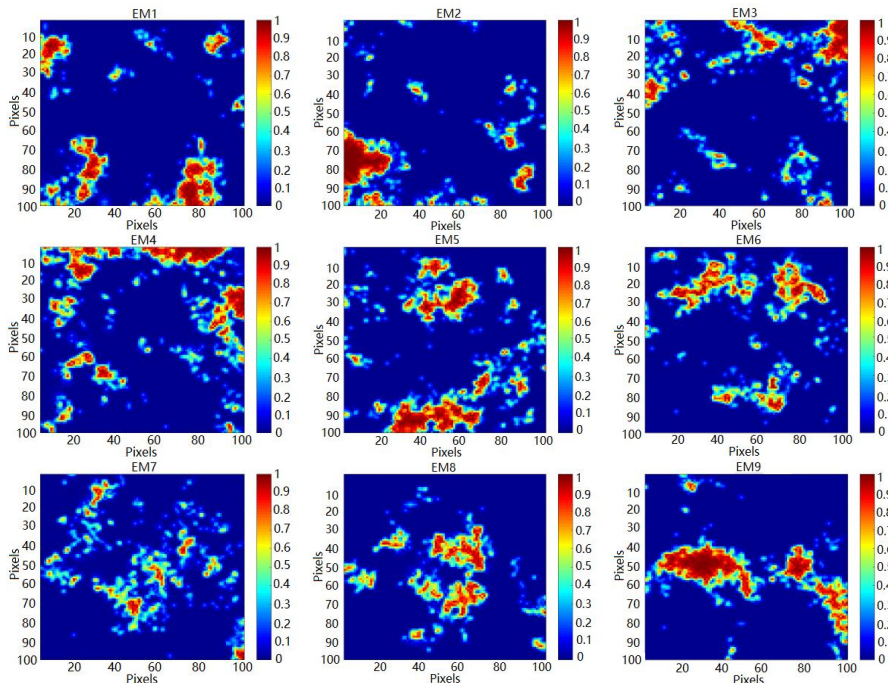


Fig. 3. True abundances of each endmembers in synthetic SD2

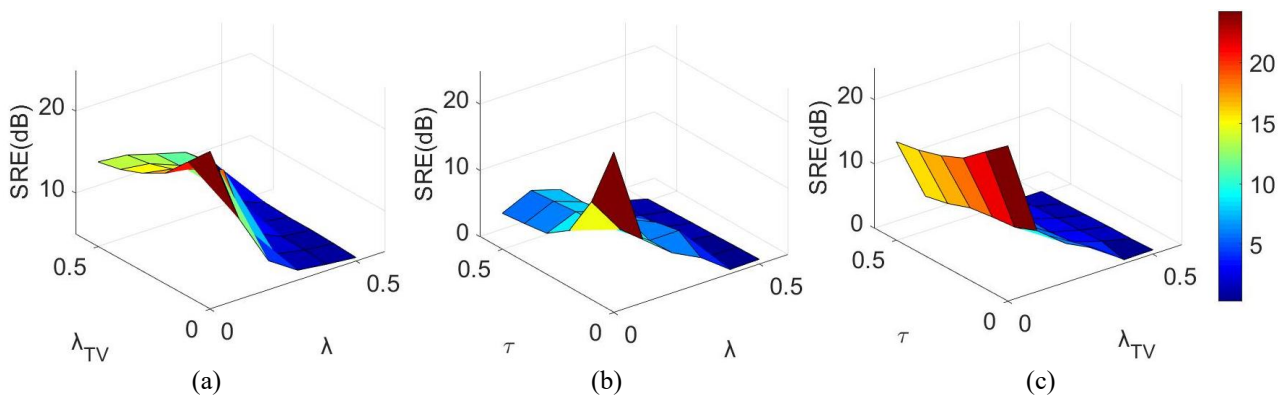


Fig. 4. SRE (dB) as a function of parameters λ , λ_{TV} and τ for DS1 at 20 dB. (a) λ and λ_{TV} . (b) λ and τ . (c) τ and λ_{TV} .

We choose the spectral library $\mathbf{A} \in \mathbb{R}^{224 \times 240}$ to unmix the synthetic datasets. \mathbf{A} is made up of the spectral curves of 240

substances randomly selected in USGS [46], each spectral curve possesses 224 bands distributed uniformly from 0.4-2.5 μm . The two synthetic hyperspectral datasets (SD1

and SD2) used in the simulation experiment are constructed from this spectral library.

1) Synthetic hyperspectral dataset 1 (SD1): The SD1 is a mixture of five randomly selected spectral curves (named endmembers) from **A** . Their corresponding abundances are different matrices of size 75*75 pixels. The fractional abundances follow the constraint of ANC and ASC. The true abundance images are shown in Fig. 2. The background of each abundance is made up by linear mixing in a 0.1149: 0.0741: 0.2003: 0.2055: 0.4051 ratio of these five endmembers.

2) Synthetic hyperspectral dataset 2 (SD2): The SD2 is also a mixture of nine randomly selected endmembers from **A** . Their corresponding abundances are different matrices of size 100*100 pixels. The fractional abundances also follow the constraint of ANC and ASC. Fig. 3 shows the true abundance images.

After these synthetic hyperspectral datasets are generated, Gaussian noise with three levels of signal-to-noise ratios (SNR) (10 dB, 20 dB and 30dB) are added to them. The results of different unmixing method after adding different noises are shown in TABLE II and TABLE III.

In order to ensure the fairness, several methods (SUnSAL-TV, SU-ATV, ADSpLRU, WNLTDUSU, LGSU, LSU, ATVWLRTSU) for comparison are uniformly iterated for 200 times to output the comparison results. In ATVWLRTSU algorithm , the two parameters (parameter k and standard deviation $\hat{\delta}$,) are only related to the synthetic datasets and have little to do with other factors. So we set $k = 15000$, $\hat{\delta} = 1.3$ in SD1 experiments, and set $k = 30000$, $\hat{\delta} = 0.3$ in SD2 experiments.

Fig. 4 shows the function diagrams of several parameters (λ , λ_{TV} , τ) and SRE for SD1 at 20dB. Since the three parameters and SRE are difficult to show in one graph, we split them into three subgraphs (λ and λ_{TV} , λ and

τ , λ_{TV} and τ). From these figures, we can find that the smaller the values of these parameters, the better the SRE .

The results of these methods are shown in TABLEs II and III, which show the optimal results (SRE, p_s , *sparsity*) and the corresponding parameters of the methods under the corresponding unmixing data and signal-to-noise ratios. In these tables, the optimal results of different algorithms are shown in bold type under the same conditions, and the sub-optimum results are shown in italic type.

From the tables II and III, we can find that SU-ATV with the addition of adaptive TV regularization term is much better than SUnSAL-TV without it, and in the SD1 data experiments, the method performance (represented by SRE) improves 42% at 10dB, 79% at 20dB and 38% at 30dB, in the SD2 data experiments, the method performance (represented by SRE) improves 14% at 10dB, 51% at 20dB and 27% at 30dB. The WNLTDUSU method using weighted low-rank tensor as a regularization term is better than the ADSpLRU using normal low-rank of matrix, and in the SD1 data experiments, the method performance (represented by SRE) improves 231% at 10dB, 261% at 20dB and 202% at 30dB, in the SD2 data experiments, the method performance (represented by SRE) improves 127% at 10dB, 102% at 20dB and 16% at 30dB. The algorithm ATVWLRTSU with both an adaptive TV regularization term and a low-rank tensor regularization term works better than these all methods (SUnSAL-TV, SU-ATV, ADSpLRU, WNLTDUSU, LGSU, LSU), and in the SD1 data experiments, the performance of the method is higher than the other algorithms 7%-256% at 10dB, 11%-300% at 20dB and 12%-238% at 30dB, in the SD2 data experiments, the performance of the method is higher than the other methods 12%-155% at 10dB, 23%-147% at 20dB and 3.5%-72% at 30dB. In particular, at low signal-to-noise ratios (e.g., 10 dB), our method still achieves 7%-255% accuracy improvement. This indicates that our method has strong denoising and robustness capabilities.

TABLE II
SRE , p_s and *sparsity* results of SD1

Algorithms	SNR=10			SNR=20			SNR=30		
	SRE	p_s	<i>sparsity</i>	SRE	p_s	<i>sparsity</i>	SRE	p_s	<i>sparsity</i>
SUnSAL-TV	5.846	0.911	0.054	8.609	0.964	0.062	16.246	<i>0.996</i>	0.037
	$\lambda=1e-1, \lambda_{TV}=2.5e-1, \mu=5e-1$			$\lambda=1.1e-2, \lambda_{TV}=7e-2, \mu=5.5e-1$			$\lambda=4e-3, \lambda_{TV}=1.5e-2, \mu=2e-1$		
SU-ATV	8.303	0.849	0.027	15.432	<i>0.994</i>	0.022	22.375	1.000	<i>0.025</i>
	$\lambda=2e-1, \lambda_{TV}=3.5e-1, \mu=1.7$			$\lambda=1.5e-2, \lambda_{TV}=1.2e-1, \mu=1.4$			$\lambda=1.8e-2, \lambda_{TV}=1.4e-2, \mu=0.3$		
ADSpLRU	4.775	0.737	0.103	6.078	0.903	0.061	10.114	0.938	0.032
	$\lambda_1=4e2, \lambda_2=3e-1, \mu=1.5$			$\lambda_1=1.2e2, \lambda_2=1e-2, \mu=1$			$\lambda_1=1.46e2, \lambda_2=4.7e-3, \mu=6.4e-1$		
WNLTDUSU	<i>15.791</i>	<i>0.995</i>	<i>0.023</i>	<i>21.916</i>	1.000	<i>0.021</i>	<i>30.5598</i>	1.000	0.020
	$\lambda=5e-2, \lambda_{TV}=1e-1, \lambda_{WT}=2.5e-2, \mu=0.5$			$\lambda=1e-3, \lambda_{TV}=5e-3, \lambda_{WT}=2.5e-3, \mu=0.5$			$\lambda=5e-6, \lambda_{TV}=2e-3, \lambda_{WT}=1e-4, \mu=0.75$		
LGSU	0.7319	0.0625	0.0912	5.678	0.7450	0.0337	13.5896	0.9981	0.0267
	$\lambda_1=3e1, \lambda_2=1e-3$			$\lambda_1=3, \lambda_2=1e-2$			$\lambda_1=8e-2, \lambda_2=3e-3$		
LSU	-0.2314	0.2425	0.0145	9.4421	0.9536	0.0215	17.8395	1	0.0219
	$\lambda=5e-3$			$\lambda=5$			$\lambda=5e-7$		
Our Method	16.951	0.999	0.021	24.3243	1.000	0.020	34.1645	1.000	0.020
	$\lambda=1e-2, \lambda_{TV}=5e-2, \tau=3e-2, \mu=2$			$\lambda=5e-4, \lambda_{TV}=1.5e-2, \tau=8e-4, \mu=1.1$			$\lambda=2e-2, \lambda_{TV}=3e-3, \tau=2e-5, \mu=8.5e-1$		

TABLE III
SRE, p_s and sparsity results of SD2

Algorithms	SNR=10			SNR=20			SNR=30		
	SRE	p_s	sparsity	SRE	p_s	sparsity	SRE	p_s	sparsity
SUnSAL-TV	3.883	0.524	0.041	6.358	0.664	0.087	11.871	0.957	0.048
	$\lambda=4e-1, \lambda_{TV}=1.4e-1, \mu=5e-1$			$\lambda=2e-2, \lambda_{TV}=1.5e-2, \mu=2.5e-2$			$\lambda=8e-3, \lambda_{TV}=4e-3, \mu=3e-2$		
SU-ATV	4.426	0.550	0.029	9.580	0.882	0.023	15.066	0.991	0.029
	$\lambda=3e-1, \lambda_{TV}=3.8e-1, \mu=1.75$			$\lambda=3e-2, \lambda_{TV}=9e-2, \mu=7e-1$			$\lambda=9e-3, \lambda_{TV}=9e-3, \mu=1.5e-1$		
ADSpLRU	2.674	0.383	0.038	4.944	0.615	0.024	12.407	0.935	0.032
	$\lambda_1=1e2, \lambda_2=3e-2, \mu=13$			$\lambda_1=19, \lambda_2=4e-2, \mu=3.3e-1$			$\lambda_1=12, \lambda_2=4e-3, \mu=6e-1$		
WNLTDUSU	6.073	0.655	0.042	9.982	0.913	0.037	14.342	0.989	0.024
	$\lambda=5e-4, \lambda_{TV}=0.1, \lambda_{WT}=2.5e-2, \mu=5e-1$			$\lambda=1e-4, \lambda_{TV}=1e-2, \lambda_{WT}=5e-4, \mu=1e-1$			$\lambda=6e-4, \lambda_{TV}=5e-3, \lambda_{WT}=2.5e-6, \mu=4e-1$		
LGSU	1.7139	0.3721	0.0443	6.8563	0.7612	0.0312	16.5564	0.9809	0.0265
	$\lambda_1=1, \lambda_2=5e-1$			$\lambda_1=5e-2, \lambda_2=1e-2$			$\lambda_1=1e-2, \lambda_2=5e-4$		
LSU	2.1526	0.3568	0.0298	9.099	0.71823	0.0285	19.7385	1	0.0242
	$\lambda=1e-3$			$\lambda=5e-3$			$\lambda=1e-2$		
Our Method	6.820	0.714	0.024	12.236	0.977	0.022	20.427	1.000	0.019
	$\lambda=2e-4, \lambda_{TV}=1e-1, \tau=8e-3, \mu=6e-1$			$\lambda=5.5e-4, \lambda_{TV}=4e-2, \tau=1e-4, \mu=5e-1$			$\lambda=1.5e-2, \lambda_{TV}=4e-4, \tau=8e-6, \mu=4e-1$		

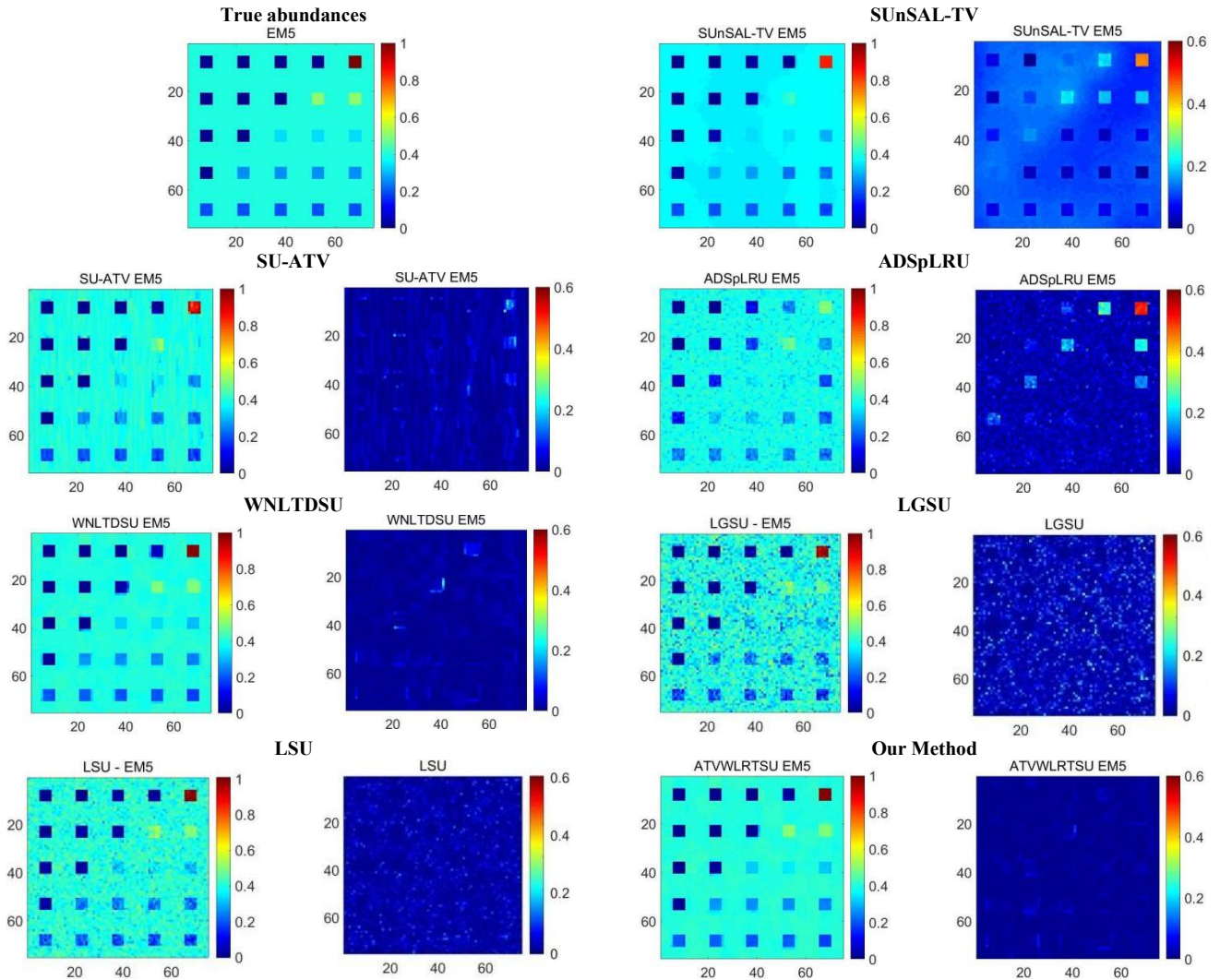


Fig. 5. True abundances of endmember5 and abundance maps estimated by these methods and the difference maps between them and true abundances at 20dB in synthetic SD1

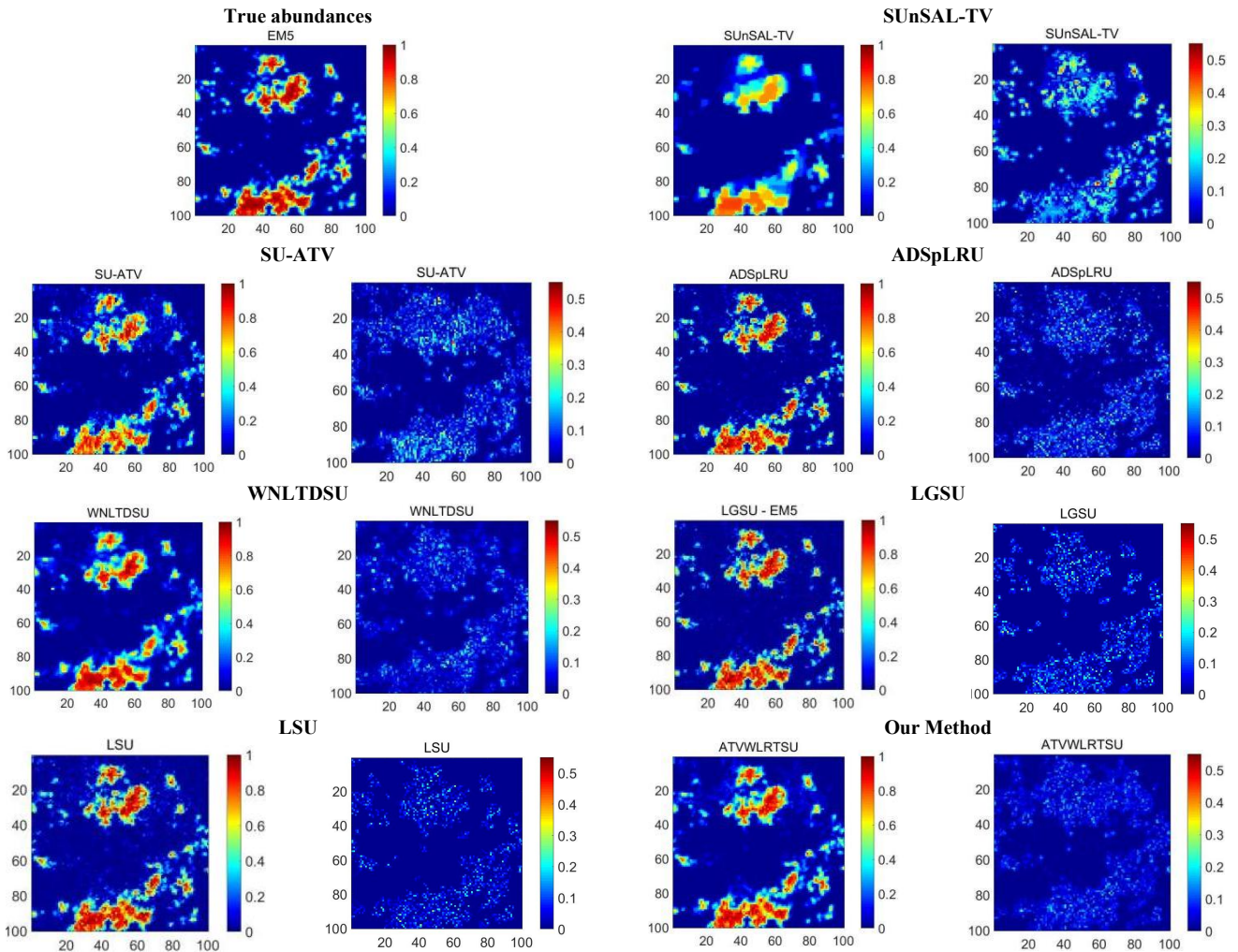


Fig. 6. True abundances of endmember5 and abundance maps estimated by these methods and the difference maps between them and true abundances at 20dB in synthetic SD2

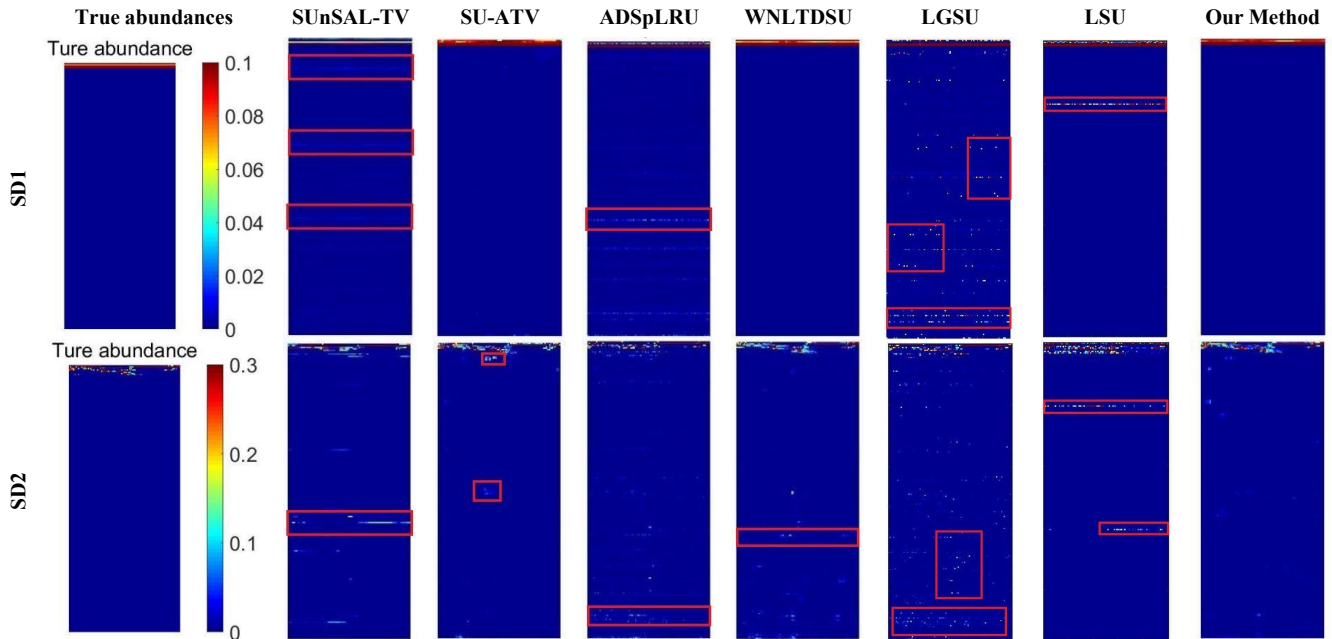


Fig. 7. True abundances (leftmost column) and abundance maps (rightmost columns) estimated by these algorithms for each endmember material in the A spectral library for 100 pixels in SD1 (topmost row) and SD2 (bottommost row) simulated with SNR of 20dB.

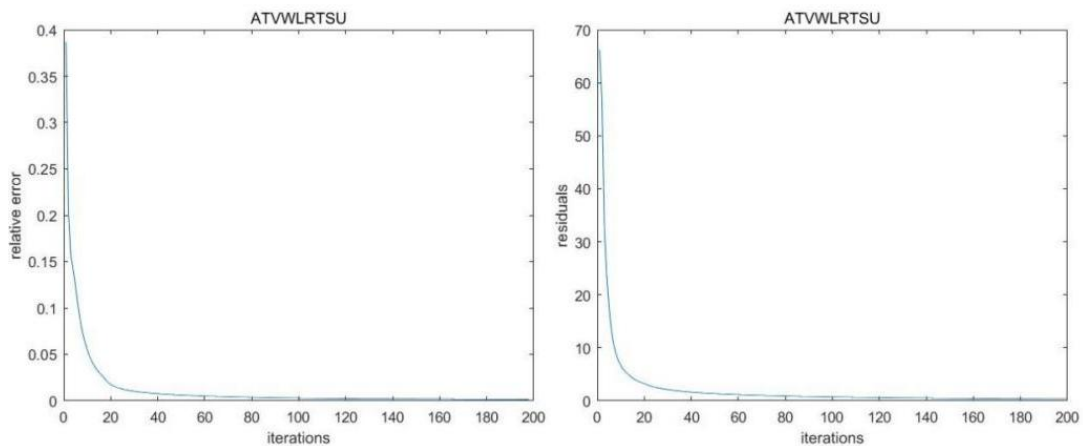


Fig. 8. The relative error and residual plots of ATVWLRTSU in SD1 simulated with SNR=20dB.

From the parameter choices of the two experiments in Tables II and III, we can see that in the high noise conditions (10dB and 20dB), parameters λ_{TV} and τ contribute more to the model solution relative to parameter λ . In the lower noise conditions (30dB), the contribution of parameters λ_{TV} and τ to the model solution is much smaller, especially for parameter τ . This indicates that under high noise conditions, there are more noise points in the data, and the sparsity effect is poor. The spatial structure information contributes significantly to the unmixing results. In the case of low noise, sparsity can achieve better results, thereby weakening the spatial information weight.

To further illustrate the superiority of the proposed method, we randomly choose an endmember (e.g. EM5) and compare the EM5's abundance images estimated by these algorithms and their differences from the true abundances at 20dB, as shown in Figs. 5 and 6. From the Fig. 5 we can see that these abundances estimated by proposed method are closest to the true abundance in SD1, followed by WNLTDUSU and SU-ATV, while the performance of LSU, SUnSAL-TV, ADSpLRU and LGSU is poor. In the Fig. 6, these abundances of SD2 estimated by proposed method are still closest to the true abundance, while WNLTDUSU, SU-ATV, LGSU, LSU and ADSpLRU have large differences, and SUnSAL-TV has poor result. Therefore our proposed method has the closest results to the true values, which is the best unmixing results.

Fig. 7. shows that the true abundance maps and approximate abundance maps estimated by these methods for each endmember material in \mathbf{A} spectral library. These experimental results are simulated with SD1 and SD2 at 20db. Due to the large number of pixels in the abundance, we randomly selected 100 pixels for display. We use this experiment to compare the unmixing results for each endmember in \mathbf{A} spectral library. Comparing with the true abundance, we can see that in the SD1 experiment, SUnSAL-TV, LGSU, LSU and ADSpLRU have explicit errors (marked in the red rectangles), while SU-ATV, WNLTDUSU and our method work better. In the SD2 experiment, except for our method, there were detailed errors in all other methods (marked in the red rectangles). These experiments have proved that the proposed method has a good unmixing effect.

Since it is difficult to verify the convergence of ATVWLRTSU, we indirectly represent the convergence of the algorithm by the relationship between residual

($\|\mathcal{V}_1^t - \mathcal{X}^t \times_3 \mathbf{A}\|$) versus the iterations and relative error ($\|\mathcal{X}^{t+1} - \mathcal{X}^t\| / \|\mathcal{X}^t\|$) versus the iterations [27]. Fig. 8 shows the residual and relative error plots of ATVWLRTSU in SD1 simulated with SNR=20dB. It can be seen in the figure that the two plots converge quickly, and the relative error is lower than 0.01 after 40 iterations, the residual is less than 1 after 60 iterations, and both values are close to 0 after 80 iterations. Therefore, it can be indirectly obtained from the figure that our proposed algorithm is convergent.

B. Experiments with real data

We use the root-mean-square error (RMSE_{RD}) and the signal-reconstruction-error of real data (SRE_{RD}) to evaluate the unmixing effect of real hyperspectral data.

$$\text{RMSE}_{\text{RD}} = \sqrt{\frac{1}{l \times n} \|\mathbf{Y} - \mathbf{A}\hat{\mathbf{X}}\|_F^2}. \quad (37)$$

$$\text{SRE}_{\text{RD}} = 10 \cdot \log_{10} [E(\|\mathbf{Y}\|_2^2) / E(\|\mathbf{Y} - \mathbf{A}\hat{\mathbf{X}}\|_2^2)]. \quad (38)$$

Lower RMSE_{RD} or Higher SRE_{RD} values mean better unmixing effect.

In this subsection, the widely used AVIRIS Cuprite dataset is used to verify the performance of the ATVWLRTSU methods. A partial subset of 250×191 pixels from the AVIRIS Cuprite dataset was chosen for the experiments. The scene consists of 224 spectral bands between 0.4 and 2.5 μm with a spectral resolution of 10 nm. The spectral library \mathbf{A} is still used for the experiments with real data. Prior to the analysis, bands 1-2, 105-115, 150-170, and 223-224 were removed from \mathbf{A} due to water absorption and low signal-to-noise ratio leaving a total of 188 spectral bands. Fig. 9 shows a mineral map produced in 1995 by USGS, in which the Tricorder 3.3 software product [47] was used to map different minerals present in the Cuprite mining district. Since the true abundances of the measured hyperspectral data are unknown, we can only qualitatively analyse their performance by comparing the mineral maps with the abundances estimated by these unmixing methods.

Fig. 10 shows the visualization comparison of the fractional abundance maps of Alunite, Buddingtonite, and Chalcedony estimated by SUnSAL-TV, SU-ATV, ADSpLRU, WNLTDUSU, LGSU, LSU and ATVWLRTSU methods using \mathbf{A} library, and the regularization parameters of these methods are shown in TABLE IV.

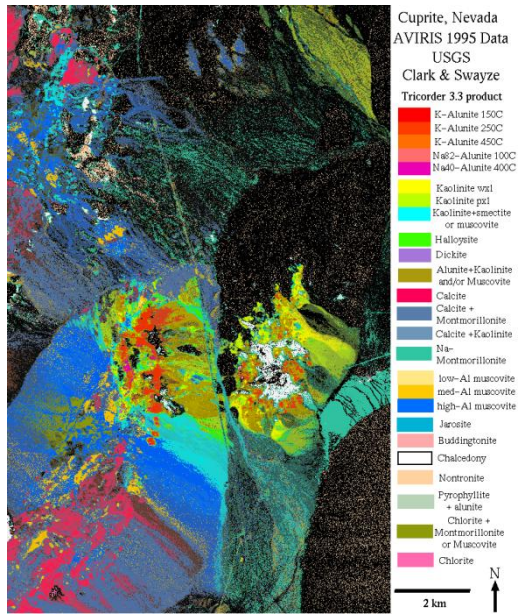


Fig. 9. USGS map showing the location of different minerals in the Cuprite mining district in Nevada.

TABLE IV
Regularization parameters of the unmixing methods

Algorithms	Regularization Parameters
SUnSAL-TV	$\lambda = 0.001, \lambda_{TV} = 0.005, \mu = 0.05$
SU-ATV	$\lambda = 0.01, \lambda_{TV} = 0.01, \mu = 0.1$
ADSpLRU	$\lambda_1 = 10, \lambda_2 = 0.005, \mu = 0.5,$
WNLTDUSU	$\lambda = 0.001, \lambda_{TV} = 0.005,$ $\lambda_{WT} = 0.00001, \mu = 0.0005$
LGSU	$\lambda_1 = 0.01, \lambda_2 = 0.005$
LSU	$\lambda = 0.01$
ATVWLRTSU	$\lambda = 0.01, \lambda_{TV} = 0.001,$ $\tau = 0.000001, \mu = 0.5$

From the results of unmixing in Fig. 10, it can be seen that the abundance maps estimated by these unmixing methods are very close to the true abundance maps. However, the abundance maps estimated by SUNSAL-TV, SU-ATV, and WNLTDUSU are too smooth (for example, the unmixing results of Chalcodony are too smooth, losing a lot of detailed information), while the abundance maps estimated by ADSpLRU are significantly different from true abundance maps (such as Buddingtonite). For Alunite mineral, the abundance maps estimated by SUNSAL-TV and SU-ATV are too smooth, and the abundance maps estimated by ADSpLRU and WNLTDUSU have some details lost. For Chalcodony mineral, the unmixing results of LGSU and LSU have larger errors. Our proposed ATVWLRTSU algorithm has good robustness and performs well in the unmixing results of three minerals. Therefore, we can conclude that the proposed ATVWLRTSU has good potential in improving

unmixing results in real scenes.

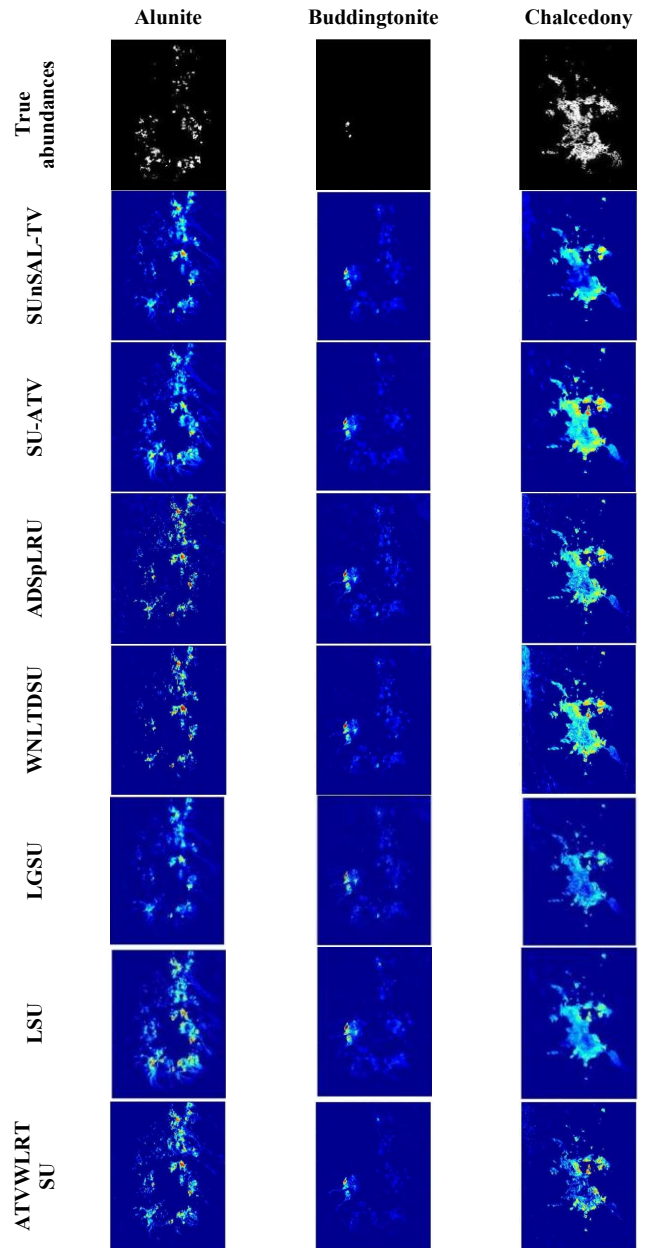


Fig. 10. Abundances of cuprite data estimated by these unmixing methods

Table V shows the quantitative comparison results used for experiments with Cuprite real hyperspectral data. From the results we can see that the algorithm proposed in this paper has the best results for both $RMSE_{RD}$ and SRE_{RD} values. This shows that the proposed algorithm has some advantages over several other algorithms.

V. CONCLUSIONS

At present, most sparse unmixing methods do not consider the spatial correlation between image features in the unmixing process. To overcome this limitation, we propose an adaptive total variation regularization for weighted low-rank tensor sparse unmixing method. This method first proposes an adaptive TV weighted term in the unmixing model to fully explore the spatial information of hyperspectral data. Then, a weighted nuclear norm of abundance tensor is introduced in unmixing model to further improve the denoising performance of the unmixing method.

Furthermore, the ADMM is used to effectively solve the proposed method. Extensive experiments on both synthetic and real data confirm the effectiveness of the proposed method, and compare with other related state-of-the-art unmixing methods, the effectiveness of the proposed method is demonstrated. The future work is the derivation of more computationally efficient schemes to further reduce computing costs.

TABLE V
RMSE_{RD} and SRE_{RD} of the unmixing methods

Algorithms	RMSE _{RD}	SRE _{RD}
SUnSAL-TV	0.0137	28.123
SU-ATV	0.0054	35.315
ADSpLRU	0.0064	31.888
WNLTDUSU	0.0052	37.117
LGSU	0.0066	31.995
LSU	0.0056	34.753
ATVWLRTSU	0.0046	39.787

REFERENCES

[1] Xin-Ru Feng, Heng-Chao Li, Rui Wang, Qian Du, Xiu-Ping Jia, and Antonio Plaza, "Hyperspectral unmixing based on nonnegative matrix factorization: A comprehensive review," *IEEE Journal of Selected Topics in Applied Earth Observations and Remote Sensing*, vol. 15, pp 4414-4436, 2022.

[2] Jian-Xin Jia, Yue-Ming Wang, Jin-Song Chen, Ran Guo, Rong Shu, and Jian-Yu Wang, "Status and application of advanced airborne hyperspectral imaging technology: A review," *Infrared Physics & Technology*, vol. 104, pp 103115, 2020.

[3] Long-Fei Ren, Dan-Feng Hong, Lian-Ru Gao, Xu Sun, Min Huang, and Jocelyn Chanussot, "Hyperspectral sparse unmixing via nonconvex shrinkage penalties," *IEEE Transactions on Geoscience and Remote Sensing*, vol. 61, pp 1-15, 2022.

[4] Lin Qi, Jie Li, Ying Wang, Yong-Fa Huang, and Xin-Bo Gao, "Spectral-spatial weighted multiview collaborative sparse unmixing for hyperspectral images," *IEEE Transactions on Geoscience and Remote Sensing*, vol. 58, no. 12, pp 8766-8779, 2020.

[5] Jiao-Jiao Wei, and Xiao-Fei Wang, "An overview on linear unmixing of hyperspectral data," *Mathematical Problems in Engineering*, vol. 2020, no. 1, pp 1-12, 2020.

[6] Preetam Ghosh, Swalpa Kumar Roy, Bikram Koirala, Behnood Rasti, and Paul Scheunders, "Hyperspectral unmixing using transformer network," *IEEE Transactions on Geoscience and Remote Sensing*, vol. 60, pp 1-16, 2022.

[7] Tao Chen, Yang Liu, Yu-Xiang Zhang, Bo Du, and Antonio Plaza, "Superpixel-based collaborative and low-rank regularization for sparse hyperspectral unmixing," *IEEE Transactions on Geoscience and Remote Sensing*, vol. 60, pp 1-16, 2022.

[8] Jie Chen, Min Zhao, Xiu-Heng Wang, Cédric Richard, and Susanto Rahardja, "Integration of physics-based and data-driven models for hyperspectral image unmixing: A summary of current methods," *IEEE Signal Processing Magazine*, vol. 40, no. 2 pp 61-74, 2023.

[9] Min Zhao, Long-Bin Yan, and Jie Chen, "LSTM-DNN based autoencoder network for nonlinear hyperspectral image unmixing," *IEEE Journal of Selected Topics in Signal Processing*, vol. 15, no. 2, pp 295-309, 2021.

[10] Lin Qi, Feng Gao, Jun-Yu Dong, Xin-Bo Gao, and Qian Du, "SSCU-Net: Spatial-spectral collaborative unmixing network for hyperspectral images," *IEEE Transactions on Geoscience and Remote Sensing*, vol. 60, pp 1-15, 2022.

[11] Qing-Le Guo, Jun-Ping Zhang, Chong-Xiao Zhong, and Ye Zhang, "Change detection for hyperspectral images via convolutional sparse analysis and temporal spectral unmixing," *IEEE Journal of Selected*

Topics in Applied Earth Observations and Remote Sensing, vol. 14, pp 4417-4426, 2021.

[12] Min Zhao, Mou Wang, Jie Chen, and Susanto Rahardja, "Hyperspectral unmixing for additive nonlinear models with a 3-D-CNN autoencoder network," *IEEE Transactions on Geoscience and Remote Sensing*, vol. 60, pp 1-15, 2021.

[13] Mohamad Dhaini, Maxime Berar, Paul Honeine, and Antonin Van Exem, "End-to-end convolutional autoencoder for nonlinear hyperspectral unmixing," *Remote Sensing*, vol. 14, no. 14, pp 3341, 2022.

[14] Jia-Feng Gu, Bin Yang, and Bin Wang, "Nonlinear unmixing for hyperspectral images via kernel-transformed bilinear mixing models," *IEEE Transactions on Geoscience and Remote Sensing*, vol. 60, pp 1-13, 2021.

[15] Farshid Khajehrayeni, and Hassan Ghassemian, "A linear hyperspectral unmixing method by means of autoencoder networks," *International Journal of Remote Sensing*, vol. 42, no. 7, pp 2517-2531, 2021.

[16] Jin-Hua Zhang, Xiao-Hua Zhang, Hong-Yun Meng, Cai-Hao Sun, Li Wang, and Xiang-Hai Cao, "Nonlinear unmixing via deep autoencoder networks for generalized bilinear model," *Remote Sensing*, vol. 14, no. 20, pp 5167, 2022.

[17] Yaser Esmaili Salehani, Ehsan Arabnejad, and Saeed Gazor, "Augmented Gaussian linear mixture model for spectral variability in hyperspectral unmixing," *IEEE International Conference on Acoustics, Speech and Signal Processing, Proceedings*, pp 1880-1884, 2021.

[18] Behnood Rasti, and Bikram Koirala, "SUNCNN: Sparse unmixing using unsupervised convolutional neural network," *IEEE Geoscience and Remote Sensing Letters*, vol. 19, pp 1-5, 2021.

[19] Mario Parente, and Marian-Daniel Iordache, "Sparse unmixing of hyperspectral data: The legacy of SUnSAL," *IEEE International Geoscience and Remote Sensing Symposium, Proceedings*, pp 21-24, 2021.

[20] Long-Fei Ren, Zheng Ma, Francesca Bovolo, Jian-Ming Hu, and Lorenzo Bruzzone, "Hyperspectral unmixing using weighted sparse regression with total variation regularization," *International Journal of Remote Sensing*, vol.43, no. 15-16, pp 6124-6151, 2022.

[21] Marian-Daniel Iordache, José M. Bioucas-Dias, and Antonio Plaza, "Sparse unmixing of hyperspectral data," *IEEE Transactions on Geoscience and Remote Sensing*, vol. 49, no. 6, pp 2014-2039, 2011.

[22] Guang-Yi Wang, You-Min Zhang, Wen-Fang Xie, Yao-Hong Qu, and Licheng Feng, "Hyperspectral linear unmixing based on collaborative sparsity and multi-band non-local total variation," *International Journal of Remote Sensing*, vol. 43, no. 1, pp 1-26, 2022.

[23] Chuan-Long Ye, Shan-Wei Liu, Ming-Ming Xu, and Zhi-Ru Yang, "Combining low-rank constraint for similar superpixels and total variation sparse unmixing for hyperspectral image," *International Journal of Remote Sensing*, vol. 43, no. 12, pp 4331-4351, 2022.

[24] Yuan Yuan, Zi-Han Zhang, and Qi Wang, "Improved collaborative non-negative matrix factorization and total variation for hyperspectral unmixing," *IEEE Journal of Selected Topics in Applied Earth Observations and Remote Sensing*, vol. 13, pp 998-1010, 2020.

[25] Xiao Li, Jie Huang, Liang-Jian Deng, and Ting-Zhu Huang, "Bilateral filter based total variation regularization for sparse hyperspectral image unmixing," *Information Sciences*, vol. 504, pp 334-353, 2019.

[26] Marian-Daniel Iordache, José M. Bioucas-Dias, and Antonio Plaza, "Total variation spatial regularization for sparse hyperspectral unmixing," *IEEE T. Geosci. Remote*, vol. 50, pp 4484-4502, 2013.

[27] Ming-Xi Ma, Chen-Guang Xu, Jun Zhang, Sheng-Qian Wang, Cheng-Zhi Deng, and Yuan-Yun Wang, "Hyperspectral sparse unmixing based on a novel adaptive total variation regularization," *Infrared Physics & Technology*, vol. 127, pp 104362, 2022.

[28] Hao Li, Ru-Yi Feng, Li-Zhe Wang, Yan-Fei Zhong, and Liang-Pei Zhang, "Superpixel-based reweighted low-rank and total variation sparse unmixing for hyperspectral remote sensing imagery," *IEEE Transactions on Geoscience and Remote Sensing*, vol. 59, no. 1, pp 629-647, 2020.

[29] Fan Li, Shao-Quan Zhang, Bing-Kun Liang, Cheng-Zhi Deng, Chen-Guang Xu, and Sheng-Qian Wang, "Hyperspectral sparse unmixing with spectral-spatial low-rank constraint," *IEEE Journal of Selected Topics in Applied Earth Observations and Remote Sensing*, vol.14, pp 6119-6130, 2021.

[30] Le Sun, Fei-Yang Wu, Tian-Ming Zhan, Wei Liu, Jin Wang, and Byeungwoo Jeon, "Weighted nonlocal low-rank tensor decomposition method for sparse unmixing of hyperspectral images," *IEEE Journal of Selected Topics in Applied Earth Observations and Remote Sensing*, vol. 13, pp 1174-1188, 2020.

[31] Lian-Ru Gao, Zhi-Cheng Wang, Li-Na Zhuang, Hao-Yang Yu, Bing Zhang, and Jocelyn Chanussot, "Using low-rank representation of abundance maps and nonnegative tensor factorization for hyperspectral

- nonlinear unmixing,” IEEE Transactions on Geoscience and Remote Sensing, vol. 60, pp 1-17, 2021.
- [32] Pan Zheng, Hong-Jun Su, and Qian Du, “Sparse and low-rank constrained tensor factorization for hyperspectral image unmixing,” IEEE Journal of Selected Topics in Applied Earth Observations and Remote Sensing, vol. 14, pp 1754-1767, 2021.
- [33] Paris V. Giampouras, Konstantinos E. Themelis, Athanasios A. Rontogiannis, and Konstantinos D. Koutroumba, “Simultaneously sparse and low-rank abundance matrix estimation for hyperspectral image unmixing,” IEEE Transactions on Geoscience and Remote Sensing, vol. 54, no. 8, pp 4775-4789, 2016.
- [34] Manyá V. Afonso, José M. Bioucas-Dias, and Mário AT Figueiredo, “An augmented Lagrangian approach to the constrained optimization formulation of imaging inverse problems,” IEEE T. Signal Proces. Vol. 20, pp 681-695, 2011.
- [35] Jie Huang, Ting-Zhu Huang, Xi-Le Zhao, and Liang-Jian Deng, “Nonlocal tensor-based sparse hyperspectral unmixing,” IEEE Transactions on Geoscience and Remote Sensing, vol.59, no. 8, 2020, pp 6854-6868.
- [36] Tales Imbiriba, Ricardo Augusto Borsoi, and José Carlos Moreira Bermudez, “Low-rank tensor modeling for hyperspectral unmixing accounting for spectral variability,” IEEE Transactions on Geoscience and Remote Sensing, vol. 58, no. 3, pp 1833-1842, 2019.
- [37] Andrzej Cichocki, Danilo Mandic, Lieven De Lathauwer, Guo-Xu Zhou, Qi-Bin Zhao, Cesar Caiafa, and Huy Anh Phan, “Tensor decompositions for signal processing applications: From two-way to multiway component analysis,” IEEE Signal Process. vol. 32, no. 2, pp 145-163, 2015.
- [38] Xin-Xin Zhang, Yuan Yuan, and Xue-Long Li, “Sparse unmixing based on adaptive loss minimization,” IEEE Transactions on Geoscience and Remote Sensing, vol. 60, pp 1-14, 2022.
- [39] Xia Xu, Bin Pan, Zong-Qing Chen, Zhen-Wei Shi, and Tao Li, “Simultaneously multiobjective sparse unmixing and library pruning for hyperspectral imagery,” IEEE Transactions on Geoscience and Remote Sensing, vol. 59, no. 4, pp 3383-3395, 2020.
- [40] Chang Li, Yu Liu, Juan Cheng, Ren-Cheng Song, Jia-Yi Ma, Chen-Hong Sui, and Xun Chen, “Sparse unmixing of hyperspectral data with bandwise model,” Information sciences, vol.512, pp 1424-1441, 2020.
- [41] Hong-Jun Su, Zhao-Yue Wu, Hui-Hui Zhang, and Qian Du, “Hyperspectral anomaly detection: A survey,” IEEE Geoscience and Remote Sensing Magazine, vol.10, no. 1, pp 64-90, 2021.
- [42] Nicolas Audebert, Bertrand Le Saux, and Sebastien Lefevre, “Deep learning for classification of hyperspectral data: A comparative review,” IEEE geoscience and remote sensing magazine, vol.7, no. 2, pp 159-173, 2019.
- [43] Zhi-Feng Pang, Hui-Li Zhang, Shou-Sheng Luo, and Tie-Yong Zeng, “Image denoising based on the adaptive weighted TVp regularization,” Signal Process, vol.167, pp 107325, 2020.
- [44] Zhi-Feng Pang, Ya-Mei Zhou, Ting-Ting Wu, and Ding-Jie Li, “Image denoising via a new anisotropic total-variation-based model,” Signal Process.-Image, vol.74, pp 140-152, 2019.
- [45] Jun Zhang, Peng-Cheng Li, Jun-Ci Yang, Ming-Xi Ma, and Cheng-Zhi Deng, “Poisson image restoration using a novel directional TVp regularization,” Signal Process. Vol.193, pp 108407, 2022.
- [46] Roger N. Clark, Gregg A. Swayze, Richard A. Wise, K. Eric Livo, Todd M. Hoefen, Raymond F. Kokaly, and Stephen J. Sutley, “USGS digital spectral library splib06a,” US Geological Survey, 2007.
- [47] Roger N. Clark, Gregg A. Swayze, K. Eric Livo, Raymond F. Kokaly, Steve J. Sutley, J. Brad Dalton, Robert R. McDougal, and Carol A. Gent, “Imaging spectroscopy: Earth and planetary remote sensing with the USGS Tetracorder and expert systems,” Journal of Geophysical Research: Planets, vol.108, pp E12, 2003.
- [48] Xiang-Fei Shen, Ha-Jun Liu, Xin-Zheng Zhang, Kai Qin, and Xi-Chuan Zhou, “Superpixel-guided local sparsity prior for hyperspectral sparse regression unmixing,” IEEE Geoscience and Remote Sensing Letters, vol.19, pp 1-5, 2022.
- [49] Xiang-Fei Shen, Li-Hui Chen, Hai-Jun Liu, Xi Su, Wen-Jia Wei, Xia Zhu, and Xi-Chuan Zhou, “Efficient hyperspectral sparse regression unmixing with multilayers,” IEEE Transactions on Geoscience and Remote Sensing, vol.61, pp 1-14, 2023.

Chenguang Xu is a lecturer of School of Information Engineering, Nanchang Institute of Technology, Nanchang, China and a PhD candidate of Intelligent Electromechanical Equipment Innovation Research Institute, East China Jiaotong University, Nanchang, China.